Published in final edited form as:
Mol Imaging Biol. 2012 February ; 14(1): 96–105. doi:10.1007/s11307-011-0479-1.

Evaluation of ^{64}Cu Labeled GX1: A Phage Display Peptide Probe for PET Imaging of Tumor Vasculature

Kai Chen[1,2], **Xilin Sun**[2], **Gang Niu**[2], **Ying Ma**[2], **Li-Peng Yap**[1], **Xiaoli Hui**[3], **Kaichun Wu**[3], **Daiming Fan**[3], **Peter S. Conti**[1], and **Xiaoyuan Chen**[2]

[1]Molecular Imaging Center, Department of Radiology, Keck School of Medicine, University of Southern California, 2250 Alcazar Street, CSC 103, Los Angeles, CA 90033-9061, USA

[2]Laboratory of Molecular Imaging and Nanomedicine (LOMIN), National Institute of Biomedical Imaging and Bioengineering (NIBIB), National Institutes of Health (NIH), 31 Center Drive, Suite 1C14, Bethesda, MD 20892-2281, USA

[3]State Key Laboratory of Cancer Biology & Institute of Digestive Diseases, Xijing Hospital, The Fourth Military Medical University, 710032, Xi'an, Shanxi, China

Abstract

Purpose—Molecular imaging using positron emission tomography (PET) radiotracers targeted to tumor vasculature offers a noninvasive method for early detection of tumor angiogenesis and efficient monitoring of response to anti-tumor vasculature therapy. The previous *in vitro* results demonstrated that the GX1 peptide, identified by phage display technology, is a tumor vasculature endothelium-specific ligand. In this study, we evaluated a ^{64}Cu-labeled GX1 peptide as a potential radiotracer for microPET imaging of tumor vasculature in a U87MG tumor xenografted mouse model.

Methods—Macrocyclic chelating agent 1,4,7,10-tetraazacyclododecane-*N*, *N*′, *N*″, *N*‴-tetraacetic acid (DOTA)-conjugated GX1 peptide was synthesized and radiolabeled with ^{64}Cu ($t_{1/2}$=12.7 h) in ammonium acetate buffer. The ^{64}Cu-labeled GX1 peptide was then subjected to *in vitro* tumor cell uptake study, small animal PET and direct tissue sampling biodistribution studies in a U87MG tumor xenografted mouse model.

Results—The *in vitro* experiment demonstrated that ^{64}Cu-DOTA-GX1 is stable in PBS with more than 91% of ^{64}Cu-DOTA-GX1 peptide remaining intact after 24 h of incubation. Cellular uptake and retention studies revealed ^{64}Cu-DOTA-GX1 binds to U87MG glioma cells and has good tumor cell retention. For small animal PET imaging studies, the U87MG tumors were all clearly visible with high contrast to contralateral background at all measured time points after injection of ^{64}Cu-DOTA-GX1 while high accumulation in liver and kidneys were also observed at early time points. The U87MG tumor uptake was determined to be the highest (7.97±0.75%ID/g) at 24 h pi. The blocking experiment was achieved by co-injection of ^{64}Cu-DOTA-GX1 with non-radiolabeled GX1 peptide (20 mg/kg) at 24 h pi, suggesting ^{64}Cu-DOTA-GX1 is a target-specific tracer. Furthermore, the biodistribution results were consistent with the quantification of microPET imaging, demonstrating the highest ratio (16.09±1.21) of tumor/muscle uptake of ^{64}Cu-DOTA-GX1 at 24 h pi for non-blocking group and significant decreased ratio (6.57±0.58) for blocking group. Finally, metabolic studies suggested that ^{64}Cu-DOTA-GX1 is stable in mouse

Correspondence to: Kai Chen; chenkai@usc.edu, Xiaoyuan Chen; shawn.chen@nih.gov.

Conflict of Interest. The authors declare that they have no conflict of interest.

blood and urine *in vivo* at early time point while the metal transchelation may also occur in mouse liver and kidneys.

Conclusion—Our studies demonstrate that ^{64}Cu-DOTA-GX1 is a promising radiotracer for imaging tumor vasculature.

Keywords

64Cu-Labeled GX1 peptide; PET imaging; Tumor vasculature; Phage display

Introduction

Molecular imaging, the visualization, characterization, and measurement of biological processes at the cellular, subcellular, and molecular level in living subjects, has rapidly gained importance in the dawning era of personalized medicine [1, 2]. As a revolutionary molecular imaging modality, positron emission tomography (PET) creates the opportunity of noninvasive quantification of diseases associated with biochemical processes [3]. Compared to morphological imaging techniques, such as computed tomography, PET requires the injection of radiotracers in the tested subject in order to acquire the imaging signal from radiotracers labeled with positron-emitting radionuclides. Therefore, discovery of biologically active PET radiotracers is of great importance for PET technology developments and their eventual impact in clinical practice.

A desirable PET probe with clinical translation potential is expected to have the following unique characteristics: (1) high binding affinity to target, (2) high specificity to target, (3) high contrast ratio, (4) good stability *in vivo*, (5) low immunogenicity and toxicity, and (6) easy production [2, 4]. To date, target-specific delivery of PET radionuclides has employed numerous targeting moieties as vehicles, including small molecules, peptides, protein, antibody and its fragments, and nanoparticle [2, 4]. Among these targeting moieties, low-molecular weight small peptides demonstrate a number of distinct advantages over others. In general, small peptides have favorable pharmacokinetic and tissue distribution patterns, as characterized by rapid clearance from blood and nontarget tissues. Some peptides have good permeability properties that can permit rapid access to target tissues. In addition, peptides usually have low toxicity and immunogenicity, and they are quite flexible in chemical modification and radiolabeling [4]. However, development of peptide-based PET radiotracers is far from trivial. An emerging technique for target-specific peptide discovery involves the screening of bacteriophage (phage) display libraries. Phage display is a powerful technique that allows vast sequence space screening, providing a means to improve peptide affinity and generate unique peptides that bind any given target [5].

Through *in vivo* screening of a phage-displayed peptide library, we previously identified a cyclic 9-mer peptide, CGNSNPKSC, named GX1, which binds specifically to the human gastric cancer vasculature [6–8]. Immunohistochemical staining, enzyme-linked immunosorbent assay (ELISA), and immunofluorescence confirmed the targeting activity of GX1 peptide, indicating that GX1 might be used as a novel vascular marker for human cancers [7, 8]. Considering tumor vasculature plays a vital role in tumor growth and metastatic spread [9, 10], development of a noninvasive imaging tool with an ability to visualize tumor vasculature in living subjects will be very useful [11]. This type of molecular probe may eventually allow us to not only early diagnose tumor angiogenesis but also accurately monitor response to anti-tumor vasculature therapy [12].

Due to the favorable nuclear characteristics of ^{64}Cu (β^+17.4% E_{max}=0.656 MeV, β^-39% E_{max}=0.573 MeV) and its availability with high specific activity, there has been considerable research interest in development of ^{64}Cu-labeled PET tracers for targeting

specific receptors [13, 14]. The half-life ($t_{1/2}$=12.7 h) of ^{64}Cu is suitable for peptide-based PET tracers, which normally require flexible radiolabeling condition and longer circulation times to achieve optimal targeting and uptake. Usually, ^{64}Cu is conjugated to targeting peptides by a chelator that is attached through a functional group [15]. The potential application of various chelating agents to the production of ^{64}Cu-labeled PET radiotracers has been previously summarized in comprehensive reviews [15–17]. Because of commercial availability of 1,4,7,10-tetraazacyclododecane-*N*,*N*′,*N*″,*N*‴-tetraacetic acid (DOTA) chelator, we chose DOTA as a chelator in this study. A GX1 analog, DOTA-conjugated GX1 peptide was synthesized and radiolabeled with a positron emitter ^{64}Cu (Fig. 1). The *in vitro* and *in vivo* stability, lipophilicity, tumor cell uptake, and retention of ^{64}Cu-DOTA-GX1 were investigated. The ability of ^{64}Cu-DOTA-GX1 to image tumor vasculature using microPET was further evaluated in a U87MG tumor xenografted mouse model.

Materials and Methods

General

All chemicals (reagent grade) were obtained from commercial suppliers and used without further purification. The Boc-protected GX1 peptide was purchased from C S Bio Company, Inc. (Menlo Park, CA, USA). DOTA-NHS-ester was purchased from Macrocyclics (Dallas, TX, USA). ^{64}Cu was produced at the National Institutes of Health by the irradiation of a thin layer of ^{64}Ni (Isoflex, USA) electroplated on a solid gold internal target plate of the CS-30 cyclotron utilizing the nuclear reaction ^{64}Ni (p,n)^{64}Cu and separated from the target material as [^{64}Cu]$CuCl_2$ by anion chromatography. Water was purified using a Milli-Q ultra-pure water system from Millipore (Milford, MA, USA), followed by passing through a Chelex 100 resin before bioconjugation and radiolabeling. Radio-TLC was performed on MKC18 silica gel 60 Å plates (Whatman, NJ, USA) with NH_4OAc-EDTA solution (2% EDTA and 10% NH_4OAc)/CH_3OH=1:1 as the eluent. The plates were read with a Bioscan AR2000 imaging scanner (Washington, DC, USA) and Winscan 2.2 software. Mass spectra were obtained on a Q-Tof premier-UPLC system equipped with an electrospray interface (ESI; Waters, USA) or a ThermoElectron Finnigan LTQ mass spectrometer equipped with an electrospray ionization source (Thermo Scientific, USA).

HPLC Methods

Analytic and semi-preparative reversed phase high-performance liquid chromatography (HPLC) were accomplished on two Waters 515 HPLC pumps, a Waters 2487 absorbance UV detector and a Ludlum Model 2200 radioactivity detector, which were operated by Waters Empower two software. The purification of DOTA-conjugated GX1 peptides were performed on a Phenomenex Luna C18 reversed phase column (5 μm, 250×10 mm). The flow rate was 3 mL/min for semi-preparative HPLC, with the mobile phase starting from 100% solvent A (0.1% trifluoroacetic acid (TFA) in water) to 25% solvent A and 75% solvent B at 28 min. The UV absorbance was monitored at 214 and 254 nm. The analytic HPLC and ^{64}Cu labeling purification were performed on a Phenomenex Luna C18 reversed phase analytic column (5 μm, 250×4.6 mm). The flow rate was 1 mL/min with the mobile phase starting from 100% solvent A (0.1% TFA in water) to 70% solvent A and 30% solvent B at 28 min. For *in vivo* stability study, analytical HPLC was operated at the same condition.

Synthesis of GX1 Peptide

Boc-protected GX1 peptide (2.0 mg, 1.988 μmol) dissolved in 1.0 mL of TFA/triisopropylsilane/water (95:2.5:2.5) solution. The mixture was stirred at room temperature for 1 h. After evaporation of solvent, the residue was redissolved in 0.5 mL of water and purified by semi-preparative HPLC. The peak containing the GX1 peptide was collected and

lyophilized to afford fluffy white powder (1.58 mg, yield: 88%). ESI-MS *m/z* $C_{33}H_{55}N_{13}O_{13}S_2$ $[M+H]^+$ calcd, 907.00; found, 907.80.

Synthesis of Boc-protected DOTA-GX1 Peptide

Boc-protected GX1 peptide (1.0 mg, 0.994 μmol) dissolved in 0.5 mL of DMF was mixed with DOTA-NHS ester(1.18 mg, 1.193 μmol) and DIPEA (10 μL). After sonicated at 45°C for 2 h, the reaction was quenched by adding 50 μL of 5% acetic acid. The solvent was removed in vacuo. The resulting residue was dissolved in acetonitrile/water (1:5) solution (containing 0.1% TFA) and purified by semi-preparative HPLC. The peak containing the Boc-protected DOTA-GX1 peptide was collected and lyophilized to afford fluffy white powder (1.2 mg, yield: 87%). ESI-HRMS *m/z* $C_{54}H_{89}N_{17}O_{22}S_2$ $[M + H]^+$ calcd, 1,393.5893; found, 1,393.7214.

Synthesis of DOTA-GX1 Peptide

Boc-protected DOTA-GX1 peptide (1.0 mg, 0.718 μmol) dissolved in 1.0 mL of TFA/triisopropylsilane/water (95:2.5:2.5) solution. The mixture was stirred at room temperature for 1 h. After evaporation of solvent, the residue was redissolved in 0.5 mL of water and purified by semi-preparative HPLC. The peak containing the DOTA-GX1 peptide was collected and lyophilized to afford fluffy white powder (0.79 mg, yield: 85%). ESI-HRMS *m/z* $C_{49}H_{81}N_{17}O_{20}S_2$ $[M+H]^+$ calcd, 1,293.5291; found, 1,293.6968.

^{64}Cu Labeling and Formulation

$[^{64}Cu]Cu(OAc)_2$ was prepared by adding 37–111 MBq of $[^{64}Cu]$ $CuCl_2$ in 0.1 N HCl into 300 μL of 0.4 M ammonium acetate buffer (pH=5.5), followed by mixing and incubating for 15 min at room temperature. The $[^{64}Cu]Cu(OAc)_2$ solution (37–111 MBq) was then added into a solution of DOTA-GX1 peptide (5 μg peptide per mCi ^{64}Cu) dissolved in 0.4 M NH_4OAc (pH=5.5) solution. The reaction mixture was incubated at 45°C for 30 min. The labeled peptide was then purified by analytical HPLC. The radioactive peak containing ^{64}Cu-labeled GX1 peptide was collected and concentrated by rotary evaporation. The product was then reconstituted in 500–800 μL phosphate-buffered saline (PBS), and passed through a 0.22-μm Millipore filter into a sterile dose vial for use in following experiments.

Partition Coefficient

The partition coefficient value was expressed as log *P*. Log *P* of ^{64}Cu-labeled GX1 peptide was determined by measuring the distribution of radioactivity in 1-octanol and PBS. Approximately 111 kBq of ^{64}Cu-labeled GX1 peptide in 2 μL of PBS (pH=7.4) was added to a vial containing 0.5 mL 1-octanol and 0.5 mL of PBS (pH=7.4). After vigorously vortexing for 10 min, the vial was centrifuged at 12,500 rpm for 5 min to ensure the complete separation of layers. 200 μL of each layer was pipetted into test tubes, and radioactivity was measured using a gamma counter (Perkin-Elmer Packard Cobra). The mean value was calculated from triplicate experiments.

Probe Stability Determination

The stability of ^{64}Cu-labeled GX1 peptide was studied at different time points. In brief, 3.7 MBq of the ^{64}Cu-labeled GX1 peptide was pipetted into 0.5 mL of PBS. After incubation at 37°C for 1, 6, and 24 h, an aliquot of the solution was removed, and the radiochemical purity was determined by HPLC.

Cell Uptake and Efflux Studies

U87MG human glioblastoma cell line was obtained from the American Type Culture Collection (Manassas, VA, USA). U87MG glioma cells were grown in Dulbecco's modified medium (USC Cell Culture Core, Los Angeles, CA, USA) supplemented with 10% fetal bovine serum at 37°C in humidified atmosphere containing 5% CO_2. The cell uptake and efflux studies were performed as previously described with some modifications [18, 19]. U87MG human glioblastoma cells were seeded into 48-well plates at a density of 2.5×10^5 cells per well 24 h prior to the experiment. U87MG cells were then incubated with ^{64}Cu-labeled GX1 peptide (370 kBq/well) at 37°C for 15, 30, 60, and 120 min. After incubation, tumor cells were washed three times with ice cold PBS and harvested by trypsinization with 0.25% trypsin/0.02% EDTA (Invitrogen, Carlsbad, CA, USA). At the end of trypsinization, wells were examined under a light microscope to ensure complete detachment of cells. Cell suspensions were collected and measured in a gamma counter (Perkin-Elmer Packard Cobra). Cell uptake data was presented as percentage of total input radioactivity after decay correction. Experiments were performed twice with triplicate wells. For efflux studies, ^{64}Cu-labeled GX1 peptide (370 kBq/well) was first incubated with U87MG cells in 48-well plates for 2 h at 37°C to allow internalization. Cells were then washed twice with PBS and incubated with cell culture medium for 15, 30, 60, and 120 min. After washing three times with PBS, cells were harvested by trypsinization with 0.25% trypsin/0.02% EDTA (Invitrogen, Carlsbad, CA, USA). Cell suspensions were collected and measured in a gamma-counter (Perkin-Elmer Packard Cobra). Experiments were done twice with triplicate wells. Cell efflux data was presented as percentage of added dose after decay correction.

Animal Model

All animal studies were approved by the Institutional Animal Care and Use Committee of Clinical Center, the National Institutes of Health. Female athymic nude mice (about 4–6 weeks old, with a body weight of 20–25 g) were obtained from Taconic Farms Inc. (Rockville, MD, USA). The U87MG human glioma xenograft model was generated by subcutaneous injection of 5×10^6 U87MG human glioma cells into the front flank of female athymic nude mice. The tumors were allowed to grow 3–5 weeks until 200–500 mm^3 in volume. Tumor growth was followed by caliper measurements of the perpendicular dimensions.

MicroPET Imaging and Blocking Experiment

MicroPET scans were performed using a rodent scanner (Inveon microPET scanner or microPET R4 scanner; Siemens Medical Solutions). About 5.55 MBq of ^{64}Cu-labeled GX1 peptide was intravenously injected into each mouse under isoflurane anesthesia. Five-minute static scans were acquired at 0.5, 1, 15, and 24 h pi, and 20-min static scan was acquired at 39 h pi. The images were reconstructed by a two-dimensional ordered-subsets expectation maximum algorithm. For each microPET scan, regions of interest were drawn over the tumor, normal tissue, and major organs on the decay-corrected whole-body coronal images. The radioactivity concentration (accumulation) within the tumor, muscle, liver, and kidneys were obtained from the mean value within the multiple regions of interest and then converted to %ID/g. For the blocking experiment, mice bearing U87MG tumors were scanned (5 min static) at 24 h after the coinjection of 5.55 MBq of ^{64}Cu-labeled GX1 peptide with 20 mg/kg GX1 peptide per mouse.

Biodistribution Studies

The U87MG tumor bearing nude mice (n=3) were injected with 7.4 MBq of ^{64}Cu-labele GX1 peptide. At 24 h after injection of the tracer, mice were sacrificed and dissected. Blood, U87MG tumor, major organs, and tissues were collected and weighed wet. The radioactivity

in the tissues was measured using a gamma counter. The results were presented as percentage injected dose per gram of tissue (%ID/g). For each mouse, the radioactivity of the tissue samples was calibrated with a known aliquot of the injected activity. Mean uptake (%ID/g) for a group of animals was calculated with standard deviations.

Metabolic Stability

The metabolic stability of ^{64}Cu-labeled GX1 peptide was evaluated in a normal athymic nude mouse. Sixty minutes after the intravenous injection of 11.1 MBq of ^{64}Cu-labeled GX1 peptide, the mouse was sacrificed, and relevant organs were harvested. The blood was collected immediately and centrifuged for 5 min at 14,000 rpm. Then, 50% TFA in 100 μL of PBS was added to the upper serum solution, followed by mixing and centrifugation for 5 min. The upper solution was taken and injected for HPLC analysis. The liver and kidneys were homogenized respectively using a homogenizer, suspended in 1 mL of PBS buffer, and then centrifuged for 5 min at 14,000 rpm. For each sample, after removal of the supernatant, 50% TFA in 100 μL PBS was added to the solution, followed by mixing and centrifugation for 5 min. The upper solution was then taken and injected for HPLC analysis. The urine sample was diluted with 1 mL PBS and passed through a C-18 cartridge. The cartridge was washed with 2 mL of water and eluted with 2 mL acetonitrile containing 0.1% TFA. After evaporation of the solvent, the residue was redissolved in 1 mL PBS. Five hundred microliter of aliquots were injected for HPLC analysis. The eluent was collected with a fraction collector (1.5 min/fraction) and the radioactivity of each fraction was measured using a gamma counter (Perkin-Elmer Packard Cobra).

Statistical Analysis

Quantitative data were expressed as mean±SD. Means were compared using one-way ANOVA and student's *t* test. *P* values <0.05 were considered statistically significant.

Results

Chemistry and Radiolabeling

The DOTA-GX1 conjugate was obtained in two steps in an overall yield of 74%. The ^{64}Cu-labeling (n=8) was achieved in more than 90% decay-corrected yield for ^{64}Cu-DOTA-GX1 with radiochemical purity of >99%. ^{64}Cu-DOTA-GX1 peptide was analyzed and purified by HPLC. The HPLC retention time of ^{64}Cu-DOTA-GX1 peptide was 13.9 min under the analytical condition. For radio-TLC analysis, the R_f values of ^{64}Cu-DOTA-GX1 was about 0.6, while the free $^{64}Cu^{2+}$ remained at the origin of TLC plate. The specific activity of ^{64}Cu-DOTA-GX1 was estimated to be about 37 MBq/nmol. The tracer was used immediately after formulation.

Log P Value and In vitro Stability

The octanol/water partition coefficient (log *P*) for ^{64}Cu-DOTA-GX1 peptide was determined to be −2.42±0.003, suggesting that ^{64}Cu-DOTA-GX1 peptide is rather hydrophilic. The *in vitro* stability of ^{64}Cu-DOTA-GX1 peptide was studied in PBS (pH 7.4) for different time intervals (1, 6, and 24 h) at physiological temperature 37°C. The stability was presented as percentage of intact ^{64}Cu-DOTA-GX1 peptide based on the HPLC analysis and the result was shown in Fig. 2. After 6 h of incubation, more than 95% of ^{64}Cu-DOTA-GX1 peptide remained intact in PBS, and more than 91% of ^{64}Cu-DOTA-GX1 peptide remained intact after 24 h of incubation.

In vitro Cell Uptake and Efflux

Cell uptake and cellular retention of ^{64}Cu-DOTA-GX1 were examined in U87MG tumor cells. The cell uptake study revealed that ^{64}Cu-DOTA-GX1 binds to U87MG tumor cells. During the first hour of incubation, about 0.1% of ^{64}Cu-DOTA-GX1 uptake in U87MG cells was determined. After 2 h incubation, the uptake of ^{64}Cu-DOTA-GX1 in U87MG cells reached the maximum of 0.29% of total input radioactivity (Fig. 3, solid line). Although the amount of ^{64}Cu-DOTA-GX1 uptake in U87MG cells was relatively low, the cell efflux study showed ^{64}Cu-DOTA-GX1 has good cell retention in U87MG cells. During 2 h of cell efflux study, only about 0.07% (from 0.29% to 0.22% of total input radioactivity) of ^{64}Cu-DOTA-GX1 efflux was determined (Fig. 3, dotted line).

MicroPET Imaging

The tumor-targeting efficacy and biodistribution pattern of ^{64}Cu-DOTA-GX1 were evaluated in nude mice bearing U87MG human glioma xenograft tumors (n=3) at multiple time points (0.5, 1, 15, 24, and 39 h) with static microPET scans. Representative decay-corrected coronal images at different time points were shown in Fig. 4a. The U87MG tumors were all clearly visible with high contrast to contralateral background at all time points measured beginning 30 min after injection of ^{64}Cu-DOTA-GX1. Predominant uptake of ^{64}Cu-DOTA-GX1 was also observed in the liver and kidneys at early time points. Tumor and major organ activity accumulation in the microPET scans was quantified by measuring the ROIs that encompassed the entire organ on the coronal images. The time–activity curves of U87MG tumor, liver, kidneys, and muscle after injection of ^{64}Cu-DOTA-GX1 were depicted in Fig. 4b. The U87MG tumor uptake of ^{64}Cu-DOTA-GX1 was calculated to be 3.01±0.53, 3.20±0.54, 5.43±0.40, 7.97±0.75, and 5.20±0.44%ID/g at 0.5, 1, 15, 24 and 39 h pi, respectively. As a function of time, the radiotracer was steadily cleared from the liver and kidneys. The live uptake values were calculated to be 17.81±0.30, 17.71±0.87, 8.86±0.50, 5.06±0.11, and 1.61± 0.16%ID/g at 0.5, 1, 15, 24 and 39 h pi, respectively. The kidney uptake values were calculated to be 17.87±0.30, 16.15 ±0.89, 7.09±0.14, 3.19±0.29, and 1.11±0.09%ID/g at 0.5, 1, 15, 24, and 39 h pi, respectively. Accumulation of the tracer in most other organs was at a very low level. As the tracer is cleared rapidly from normal nontargeted organs, the tumor/nontarget (T/NT) ratio increased with time. The highest contrast ratio of tumor to background was reached at 24 h pi.

Blocking Experiment

The target specificity of ^{64}Cu-DOTA-GX1 was achieved by a blocking experiment where the tracer was co-injected with GX1 peptide (20 mg/kg of mouse body weight). Illustrated in Fig. 5a are the representative coronal images of U87MG tumor-bearing mice at 24 h pi of ^{64}Cu-DOTA-GX1 with and without coinjection of GX1 peptide (20 mg/kg). The quantitative analyses of microPET imaging of U87MG tumor, muscle, liver and kidneys were shown in Fig. 5b. The U87MG tumor uptake in the presence of non-radiolabeled GX1 peptide (2.31±0.08%ID/g) was significantly lower than that without GX1 blocking (7.97±0.75%ID/g; P<0.01) at 24 h pi. The presence of non-radiolabled GX1 peptide also decreased the uptake of ^{64}Cu-DOTA-GX1 in liver and kidneys whereas the uptake of ^{64}Cu-DOTA-GX1 in muscle minimally altered between control and blocking group.

Biodistribution Studies

The *in vivo* biodistribution of ^{64}Cu-DOTA-GX1 was examined in U87MG tumor-bearing mice at 24 h pi with and without coinjection of non-radiolabeled GX1 peptide (20 mg/kg of mouse body weight). The percentage administered activity (injected dose) per gram of tissue (%ID/g) was shown in Fig. 6a. The biodistribution results were consistent with the quantification of microPET imaging. At 24 h pi, the U87MG tumor uptake of ^{64}Cu-DOTA-

GX1 was reached to 6.46±0.29%ID/g whereas the presence of non-labeled GX1 peptide significantly reduced the tumor uptake to 2.31±0.07%ID/g (P<0.01) in blocking group. In addition, ^{64}Cu-DOTA-GX1 peptide displayed high accumulation and retention in liver and kidneys at 24 h pi. For non-blocking group, 5.03±0.14 and 3.25±0.24%ID/g was remained in liver and kidneys, respectively. Furthermore, similar to microPET imaging analyses, the presence of non-radiolabled GX1 peptide decreased the overall uptake of ^{64}Cu-DOTA-GX1 in most tissues and organs. Based on the biodistribution results, the contrast ratios of tumor to normal organs for non-blocking and blocking group were calculated and presented in Fig. 6b. For non-blocking group, the ratio of tumor uptake to muscle, liver, and kidney uptake at 24 pi was calculated to be 16.09±1.21, 1.29±0.05, 3.98±0.66, respectively; while the corresponding values for blocking group were 6.57±0.58, 0.88±0.10, 1.42± 0.19, respectively.

Metabolic Stability of ^{64}Cu-Labeled GX1 Peptide

The metabolic stability of ^{64}Cu-DOTA-GX1 was determined in mouse blood, urine, liver, and kidneys at 1 h after intravenous injection of radiotracer into a normal athymic nude mouse. The radioactivity of each sample was analyzed by HPLC and the representative data were listed in Table 1. The amount of intact ^{64}Cu-DOTA-GX1 tracer in blood, urine, liver, and kidneys were approximately 75%, 82%, 38%, and 64%, respectively.

Discussion

PET is one of the most rapidly growing areas of medical imaging, with many applications in the clinical management of patients with cancer. PET imaging takes advantage of the traditional diagnostic imaging techniques and introduces positron-emitting probes to determine the expression of indicative molecular targets at different stages of cancer disease [20]. 2-deoxy-2-[^{18}F]fluoro-D-glucose ([^{18}F]FDG) is the most widely used PET radiotracer in oncology. After administration of [^{18}F]FDG into the body, it is taken up into various tissues and trapped intracellularly. In fact, increased glucose transport is associated with elevated glycolysis of the cancer cell and a corresponding increase in hexokinase activity. However, [^{18}F]FDG is not a target-specific tracer and it cannot differentiate between cells that have a high metabolic rate associated with neoplasia, and those for which the increased metabolic rate is associated with other etiologies, such as infection or inflammation. Over the past decade, alternative PET radiotracers to [^{18}F]FDG that target specific biological process in cancer biology have been extensively explored. It is worth to note that development of a PET radiotracer is unlikely to be successful unless the molecular target is well defined and its biological role is well characterized. It is fortunate that the outcomes of biomedical research have yielded an enormous amount of information about the molecular events that take place during the development of cancer.

Angiogenesis, the formation of new blood vessels from pre-existing vasculature, is a fundamental process occurring during tumor progression [9, 20]. A sizable body of evidence suggests tumor–vasculature formation is a complex multi-step process that follows a characteristic sequence of events mediated and controlled by growth factors, cellular receptors, and adhesion molecules [21–23]. Differences between tumor angiogenesis and physiological angiogenesis include aberrant vascular structure, altered endothelial cell-pericyte interactions, abnormal blood flow, increased permeability, and delayed maturation [24, 25]. Because tumor vasculature plays a vital role in tumor growth and metastasis, it is important to develop a PET molecular probe for imaging tumor vasculature in living subjects, which will allow us to early detect tumor angiogenesis as well as accurately monitor response of tumor vasculature to therapy.

Phage display technology is a powerful approach for the generation of peptides that target specific organ or tumor structures [26]. Since its inception almost 30 years ago, phage display has been utilized *in vitro*, *in situ*, and *in vivo* to isolate peptides that bind numerous targets [5]. Through *in vivo* screening of a phage-displayed peptide library, we previously identified a cyclic 9-mer peptide, CGNSNPKSC, named GX1, which binds specifically to the human gastric cancer vasculature [6–8]. Although the identification of specific target receptor for GX1 peptide is underway, the results from immunohistochemical staining, ELISA, and immunofluorescence indicate that GX1 might be used as a novel vascular marker for human cancers [7, 8]. Considering all of above factors, we hypothesized that radiolabeling GX1 peptide would generate a novel radiotracer for PET imaging of tumor vasculature.

Subsequently, GX1 peptide was conjugated with DOTA and radiolabeled with ^{64}Cu. The resulting ^{64}Cu-DOTA-GX1 tracer was evaluated *in vitro* and *in vivo* for imaging tumor vasculature. The *in vitro* experiment demonstrated that ^{64}Cu-DOTA-GX1 is stable in PBS with more than 91% of ^{64}Cu-DOTA-GX1 peptide remaining intact after 24 h of incubation. Utilization of U87MG cells for cell uptake study was performed considering that these tumor cells represent the bulk of the mass in the xenograft. As vasculature formation in glioblastoma multiforme is disorganized and highly permeable [27], it is reasonable to assume that most vasculature targeting will result in leakage of the radiotracer into surrounding cellular milieu. Cellular uptake study revealed that ^{64}Cu-DOTA-GX1 binds to U87MG glioma cells and the uptake can be reached at 0.29% of total input radioactivity after 2 h incubation. Significant increase of ^{64}Cu-DOTA-GX1 uptake in U87MG cells was observed after 1 h incubation as shown in Fig. 3. One possible explanation for this phenomenon is that GX1 could be internalized into U87MG cells as a function of incubation time. Actually, Cy5.5-GX1 conjugation has been prepared and the U87MG cell uptake of Cy5.5-GX1 has been examined by a confocal microscopy. The results showed Cy5.5-GX1 was indeed internalized into the U87MG cells (data not shown). Furthermore, a cellular retention study demonstrated that ^{64}Cu-DOTA-GX1 is slowly washed out from cells, with 76% of the radioactivity still associated with the cells after 2 h incubation. These *in vitro* results justified its further evaluation in animal models. MicroPET imaging and quantification analysis of ^{64}Cu-DOTA-GX1 in mice bearing U87MG tumor at 0.5, 1, 15, and 24 h after tail veil injection showed high U87MG tumor-to-background. Accumulation of ^{64}Cu-DOTA-GX1 is mainly in tumor, liver, and kidneys while the tracer uptake in most other organs is at a very low level. As the tracer is cleared rapidly from normal nontargeted organs, the T/NT ratio is increased along the time. The target specificity of ^{64}Cu-DOTA-GX1 was achieved by a blocking experiment where the tracer was co-injected with non-radiolabeled GX1 peptide. The U87MG tumor uptake for blocking group was significantly lower than that for non-blocking group, indicating ^{64}Cu-DOTA-GX1 is a target-specific tracer. The results from *in vivo* biodistribution studies are consistent with the findings obtained from microPET imaging. At 24 h pi, the U87MG tumor uptake of ^{64}Cu-DOTA-GX1 for non-blocking group can be reached to 6.46±0.29%ID/g and tumor-to-muscle ratio is as high as 16. Co-injection of ^{64}Cu-DOTA-GX1 with non-radiolabled GX1 peptide decreased the tracer uptake in U87MG tumor as well as in most tissues and organs.

For ^{64}Cu labeling, DOTA was previously reported as a widely used “universal” chelator, and we have reported a series of ^{64}Cu-DOTA peptide tracers for tumor imaging [28–32]. The high and prolonged liver uptake is problematic for ^{64}Cu-DOTA radiotracers, which was suggested to be the slow dissociation of ^{64}Cu from the DOTA chelator [33]. The instability of the ^{64}Cu-DOTA conjugates would result in demetalation and subsequent accumulation in nontarget tissues and organs such as in the liver. In this study, high accumulation and retention of ^{64}Cu-DOTA-GX1 in the liver were also observed in both microPET imaging and biodistribution studies (Figs. 4 and 6). Better chelation systems for ^{64}Cu labeling such

as TETA (1,4,8,11-tetraazacyclotetradecane-*N*, *N*′, *N*″, *N*‴-tetraacetic acid), cross-bridged cyclam ligands, and sarcophagine (3,6,10,13,16,19-hexaazabicyclo[6.6.6]icosane) may improve the metal–chelate stability and subsequently lead to better pharmacokinetic profile [33–36]. In addition, it is well-documented that an appropriate linker has a profound impact on the biodistribution of imaging probes [37–39]. Thus, an appropriate linker may be incorporated into GX1 tracer to further orchestrate its favorable pharmacokinetics. The factor of length, flexibility, hydrophilicity, and charges (cationic, anionic, and neutral) of the linker needs to be considered to provide better somatic contrasts from the imaging perspective.

Conclusion

The radiosynthesis of ^{64}Cu-DOTA-GX1 tracer was achieved in high yield under mild condition. ^{64}Cu-DOTA-GX1 exhibits good cell uptake, internalization, and retention in U87MG glioma cells. microPET imaging and biodistribution studies demonstrate excellent tumor-targeting efficacy and specificity of ^{64}Cu-DOTA-GX1 in U87MG xenograft mouse model. ^{64}Cu-DOTA-GX1 peptide is a promising radiotracer for imaging tumor vasculature in living subjects.

Acknowledgments

This study was supported in part by the Intramural Research Program of the National Institute of Biomedical Imaging and Bioengineering (NIBIB), National Institutes of Health, the USC Department of Radiology, and the Provost's Biomedical Imaging Science Initiative.

Abbreviations

PET	positron emission tomography
HPLC	high-performance liquid chromatography
TLC	thin-layer chromatography
%ID/g	percentage injected dose per gram of tissue
pi	postinjection
GX1	cyclo(CGNSNPKSC) peptide
PBS	phosphate-buffered saline
DOTA	1,4,7,10-tetraazacyclododecane-*N*, *N*′, *N*″, *N*‴-tetraacetic acid
Boc	*t*-butoxycarbonyl
NHS	*N*-hydroxysuccinimide
TFA	trifluoroacetic acid
EDTA	ethylenediaminetetraacetic acid
DMF	*N*,*N*-dimethylformamide
DIPEA	diisopropylethylamine

References

1. Weissleder R, Mahmood U. Molecular imaging. Radiology. 2001; 219:316–333. [PubMed: 11323453]
2. Chen K, Chen X. Design and development of molecular imaging probes. Curr Top Med Chem. 2010; 10:1227–1236. [PubMed: 20388106]

3. Massoud TF, Gambhir SS. Molecular imaging in living subjects: seeing fundamental biological processes in a new light. Genes Dev. 2003; 17:545–580. [PubMed: 12629038]
4. Chen K, Conti PS. Target-specific delivery of peptide-based probes for PET imaging. Adv Drug Deliv Rev. 2010; 62:1005–1022. [PubMed: 20851156]
5. Deutscher SL. Phage display in molecular imaging and diagnosis of cancer. Chem Rev. 2010; 110:3196–3211. [PubMed: 20170129]
6. Chen B, Cao S, Zhang Y, Wang X, Liu J, Hui X, Wan Y, Du W, Wang L, Wu K, Fan D. A novel peptide (GX1) homing to gastric cancer vasculature inhibits angiogenesis and cooperates with TNF alpha in anti-tumor therapy. BMC Cell Biol. 2009; 10:63. [PubMed: 19740430]
7. Zhi M, Wu KC, Dong L, Hao ZM, Deng TZ, Hong L, Liang SH, Zhao PT, Qiao TD, Wang Y, Xu X, Fan DM. Characterization of a specific phage-displayed peptide binding to vasculature of human gastric cancer. Cancer Biol Ther. 2004; 3:1232–1235. [PubMed: 15492500]
8. Hui X, Han Y, Liang S, Liu Z, Liu J, Hong L, Zhao L, He L, Cao S, Chen B, Yan K, Jin B, Chai N, Wang J, Wu K, Fan D. Specific targeting of the vasculature of gastric cancer by a new tumor-homing peptide CGNSNPKSC. J Control Release. 2008; 131:86–93. [PubMed: 18700158]
9. Cai W, Gambhir SS, Chen X. Chapter 7. Molecular imaging of tumor vasculature. Methods Enzymol. 2008; 445:141–176. [PubMed: 19022059]
10. Weissleder R. Molecular imaging in cancer. Science. 2006; 312:1168–1171. [PubMed: 16728630]
11. Weissleder R. Scaling down imaging: molecular mapping of cancer in mice. Nat Rev Cancer. 2002; 2:11–18. [PubMed: 11902581]
12. Cai W, Rao J, Gambhir SS, Chen X. How molecular imaging is speeding up antiangiogenic drug development. Mol Cancer Ther. 2006; 5:2624–2633. [PubMed: 17121909]
13. Blower PJ, Lewis JS, Zweit J. Copper radionuclides and radiopharmaceuticals in nuclear medicine. Nucl Med Biol. 1996; 23:957–980. [PubMed: 9004284]
14. Liu S. Bifunctional coupling agents for radiolabeling of biomolecules and target-specific delivery of metallic radionuclides. Adv Drug Deliv Rev. 2008; 60:1347–1370. [PubMed: 18538888]
15. Sun X, Anderson CJ. Production and applications of copper-64 radiopharmaceuticals. Methods Enzymol. 2004; 386:237–261. [PubMed: 15120255]
16. Anderson CJ, Ferdani R. Copper-64 radiopharmaceuticals for PET imaging of cancer: advances in preclinical and clinical research. Cancer Biother Radiopharm. 2009; 24:379–393. [PubMed: 19694573]
17. Shokeen M, Anderson CJ. Molecular imaging of cancer with copper-64 radiopharmaceuticals and positron emission tomography (PET). Acc Chem Res. 2009; 42:832–841. [PubMed: 19530674]
18. Liu Z, Niu G, Wang F, Chen X. (68)Ga-labeled NOTA-RGD-BBN peptide for dual integrin and GRPR-targeted tumor imaging. Eur J Nucl Med Mol Imaging. 2009; 36:1483–1494. [PubMed: 19360404]
19. Sun X, Niu G, Yan Y, Yang M, Chen K, Ma Y, Chan N, Shen B, Chen X. Phage display-derived peptides for osteosarcoma imaging. Clin Cancer Res. 2010; 16:4268–4277. [PubMed: 20570932]
20. Chen K, Chen X. PET Imaging of cancer biology: current status and future prospects. Semin Oncol. 2011; 38:70–86. [PubMed: 21362517]
21. Ellis LM, Liu W, Ahmad SA, Fan F, Jung YD, Shaheen RM, Reinmuth N. Overview of angiogenesis: biologic implications for anti-angiogenic therapy. Semin Oncol. 2001; 28:94–104. [PubMed: 11706401]
22. Kuwano M, Fukushi J, Okamoto M, Nishie A, Goto H, Ishibashi T, Ono M. Angiogenesis factors. Intern Med. 2001; 40:565–572. [PubMed: 11506294]
23. Yancopoulos GD, Davis S, Gale NW, Rudge JS, Wiegand SJ, Holash J. Vascular-specific growth factors and blood vessel formation. Nature. 2000; 407:242–248. [PubMed: 11001067]
24. Bergers G, Benjamin LE. Tumorigenesis and the angiogenic switch. Nat Rev Cancer. 2003; 3:401–410. [PubMed: 12778130]
25. Hanahan D, Folkman J. Patterns and emerging mechanisms of the angiogenic switch during tumorigenesis. Cell. 1996; 86:353–364. [PubMed: 8756718]

26. Ueberberg S, Schneider S. Phage library-screening: a powerful approach for generation of targeting-agents specific for normal pancreatic islet-cells and islet-cell carcinoma *in vivo*. Regul Pept. 2010; 160:1–8. [PubMed: 19958795]
27. Soda Y, Marumoto T, Friedmann-Morvinski D, Soda M, Liu F, Michiue H, Pastorino S, Yang M, Hoffman RM, Kesari S, Verma IM. Feature article: transdifferentiation of glioblastoma cells into vascular endothelial cells. Proc Natl Acad Sci U S A. 2011 (in press).
28. Chen X, Park R, Hou Y, Tohme M, Shahinian AH, Bading JR, Conti PS. microPET and autoradiographic imaging of GRP receptor expression with 64Cu-DOTA-[Lys3]bombesin in human prostate adenocarcinoma xenografts. J Nucl Med. 2004; 45:1390–1397. [PubMed: 15299066]
29. Wu Y, Zhang X, Xiong Z, Cheng Z, Fisher DR, Liu S, Gambhir SS, Chen X. microPET imaging of glioma integrin {alpha}v{beta}3 expression using (64)Cu-labeled tetrameric RGD peptide. J Nucl Med. 2005; 46:1707–1718. [PubMed: 16204722]
30. Li ZB, Cai W, Cao Q, Chen K, Wu Z, He L, Chen X. (64)Cu-labeled tetrameric and octameric RGD peptides for small-animal PET of tumor alpha(v)beta(3) integrin expression. J Nucl Med. 2007; 48:1162–1171. [PubMed: 17574975]
31. Cai W, Wu Y, Chen K, Cao Q, Tice DA, Chen X. *In vitro* and *in vivo* characterization of 64Cu-labeled Abegrin, a humanized monoclonal antibody against integrin alpha v beta 3. Cancer Res. 2006; 66:9673–9681. [PubMed: 17018625]
32. Chen X, Liu S, Hou Y, Tohme M, Park R, Bading JR, Conti PS. MicroPET imaging of breast cancer alphav-integrin expression with 64Cu-labeled dimeric RGD peptides. Mol Imaging Biol. 2004; 6:350–359. [PubMed: 15380745]
33. Boswell CA, Sun X, Niu W, Weisman GR, Wong EH, Rheingold AL, Anderson CJ. Comparative *in vivo* stability of copper-64-labeled cross-bridged and conventional tetraazamacrocyclic complexes. J Med Chem. 2004; 47:1465–1474. [PubMed: 14998334]
34. Sun X, Wuest M, Weisman GR, Wong EH, Reed DP, Boswell CA, Motekaitis R, Martell AE, Welch MJ, Anderson CJ. Radiolabeling and *in vivo* behavior of copper-64-labeled cross-bridged cyclam ligands. J Med Chem. 2002; 45:469–477. [PubMed: 11784151]
35. Cai H, Li Z, Huang CW, Shahinian AH, Wang H, Park R, Conti PS. Evaluation of copper-64 labeled AmBaSar conjugated cyclic RGD peptide for improved MicroPET imaging of integrin alphavbeta3 expression. Bioconjug Chem. 2010; 21:1417–1424. [PubMed: 20666401]
36. Cai H, Li Z, Huang CW, Park R, Shahinian AH, Conti PS. An improved synthesis and biological evaluation of a new cage-like bifunctional chelator, 4-((8-amino-3, 6, 10, 13, 16, 19-hexaazabicyclo [6.6.6]icosane-1-ylamino)methyl)benzoic acid, for 64Cu radiopharmaceuticals. Nucl Med Biol. 2010; 37:57–65. [PubMed: 20122669]
37. Chen X. Multimodality imaging of tumor integrin alphavbeta3 expression. Mini Rev Med Chem. 2006; 6:227–234. [PubMed: 16472190]
38. Haubner R, Wester HJ, Weber WA, Mang C, Ziegler SI, Goodman SL, Senekowitsch-Schmidtke R, Kessler H, Schwaiger M. Non-invasive imaging of alpha(v)beta3 integrin expression using 18 F-labeled RGD-containing glycopeptide and positron emission tomography. Cancer Res. 2001; 61:1781–1785. [PubMed: 11280722]
39. Shi J, Kim YS, Zhai S, Liu Z, Chen X, Liu S. Improving tumor uptake and pharmacokinetics of (64)Cu-labeled cyclic RGD peptide dimers with Gly(3) and PEG(4) linkers. Bioconjug Chem. 2009; 20:750–759. [PubMed: 19320477]

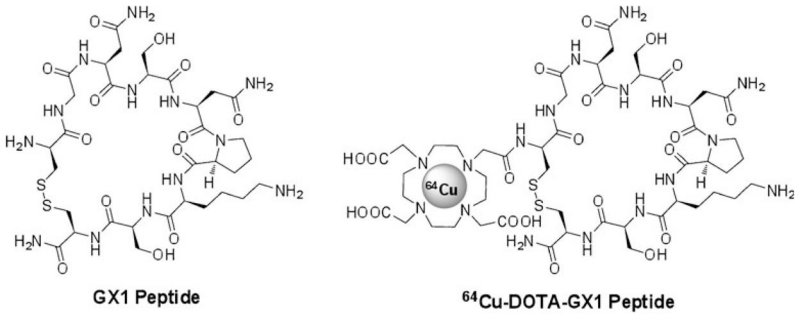

Fig. 1.
Chemical structure of GX1 peptide and ^{64}Cu-DOTA-GX1 peptide.

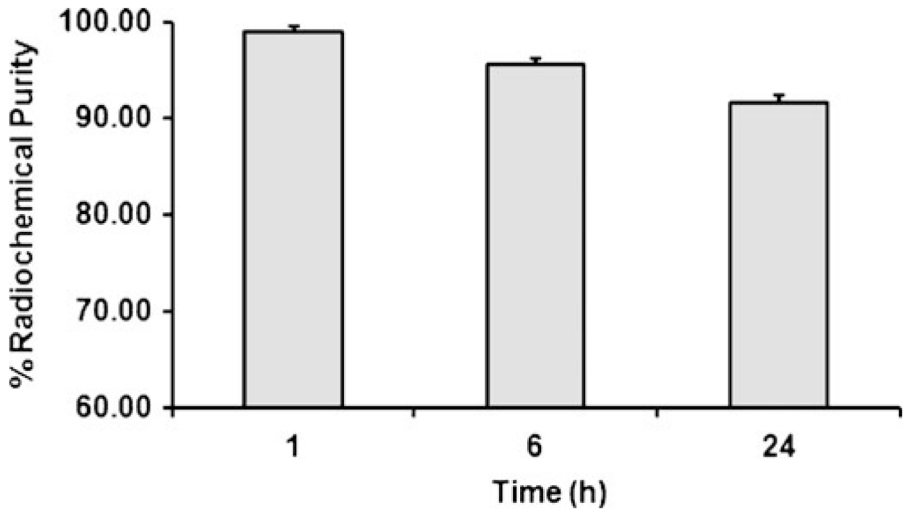

Fig. 2.
Stability of ^{64}Cu-DOTA-GX1 peptide in PBS (pH=7.4) at 37°C for 1, 6, and 24 h.

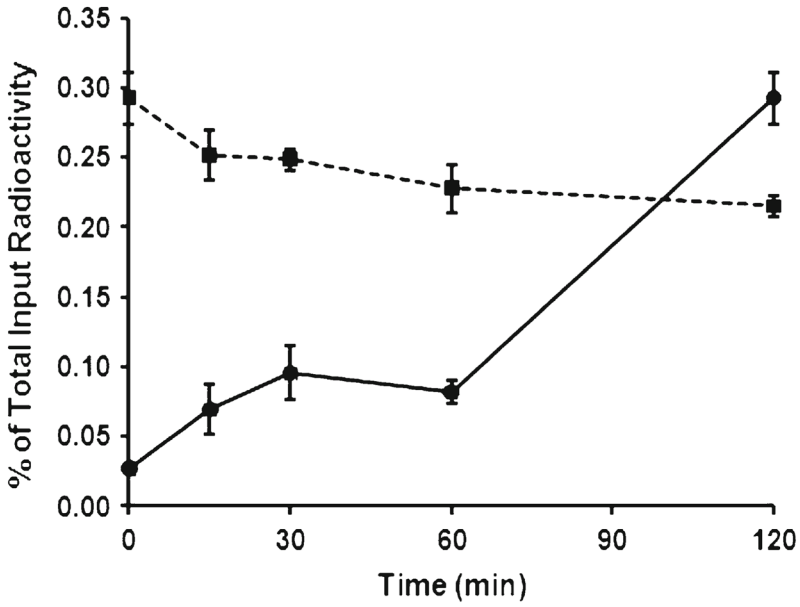

Fig. 3.

Cell uptake and efflux assay. *Solid line* time-dependent uptake of ^{64}Cu-DOTA-GX1 in U87MG cells (n=3, mean± SD). The background readings are reflected at time 0. *Dotted line* time-dependent efflux of ^{64}Cu-DOTA-GX1 in U87MG cells (n=3, mean±SD).

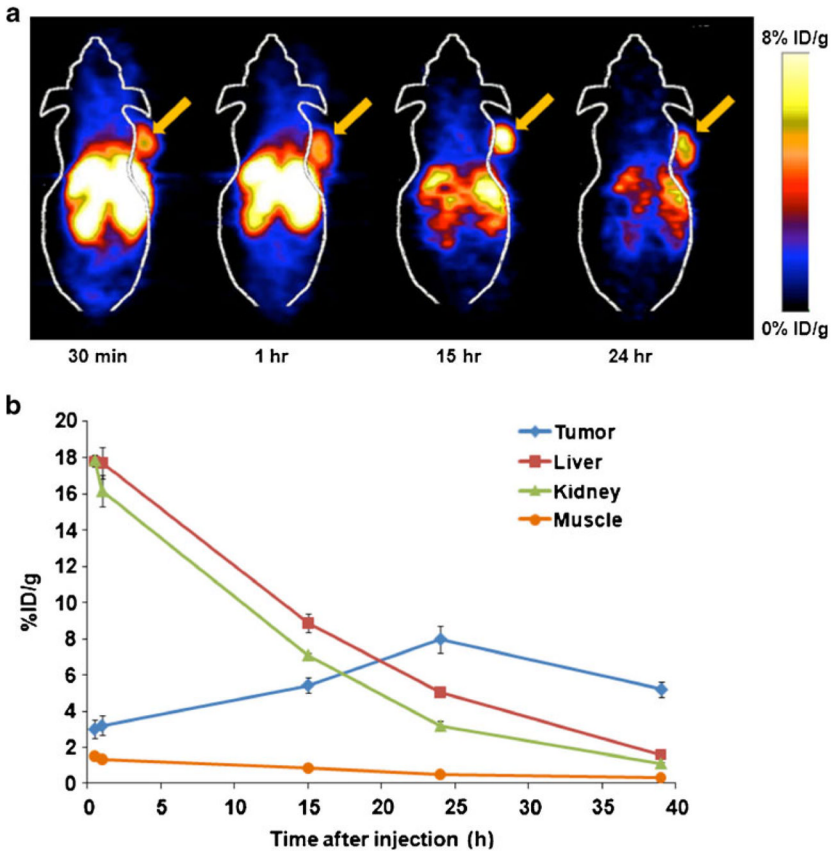

Fig. 4.

MicroPET study of subcutaneous U87MG tumor-bearing nude mice after intravenous (i.v.) injection of 5.55 MBq of ^{64}Cu-DOTA-GX1 peptide. **a** Decay-corrected whole-body coronal microPET images of nude mice bearing U87MG tumor at 0.5, 1, 15, and 24 h pi. Tumors are indicated by *arrows*. **b** Time–activity curves of U87MG tumor, liver, kidney, and muscle. ROIs are shown as the mean%ID/g±SD (n=3/group).

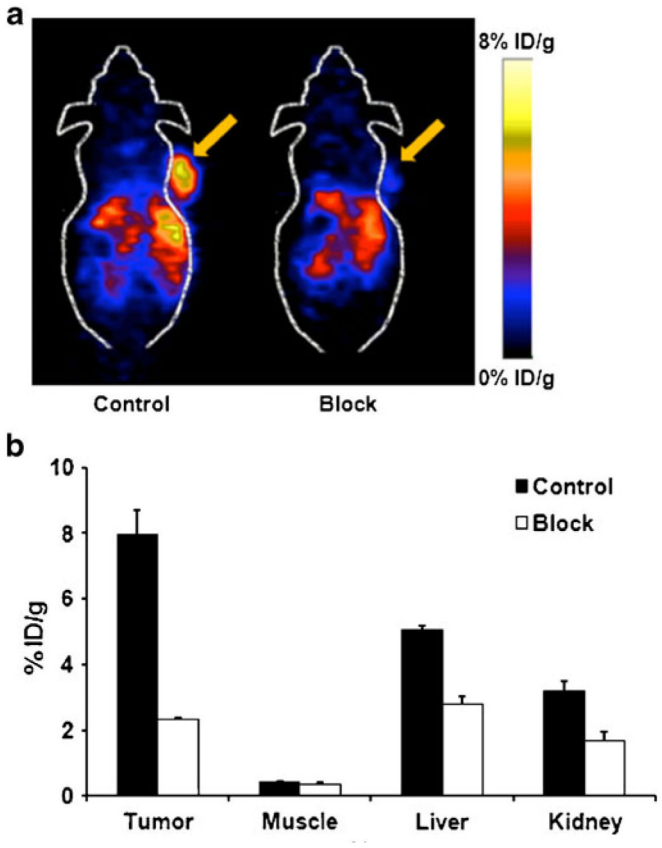

Fig. 5.

MicroPET imaging of ^{64}Cu-DOTA-GX1 in U87MG tumor bearing athymic nude mice at 24 h with and without co-injection of 20 mg/kg of GX1 peptide as a blocking agent (n=3/group). **a** Decay-corrected whole-body coronal micro-PET images. Tumors are indicated by arrows. **b** Quantitative analyses of microPET imaging of U87MG tumor, muscle, liver, and kidney (n=3/group).

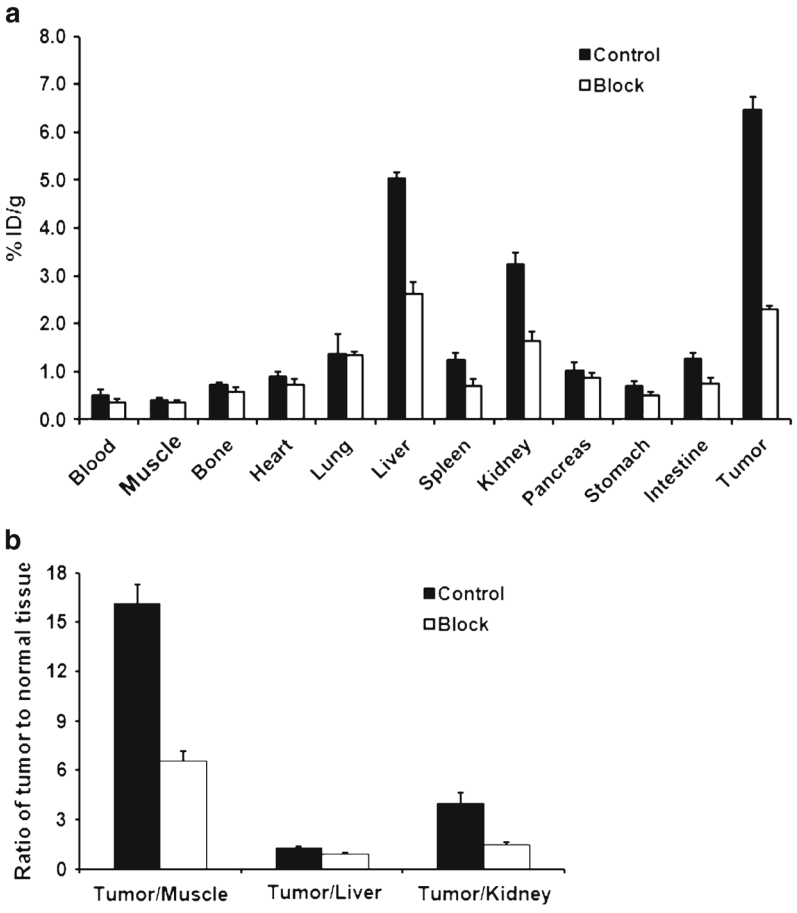

Fig. 6.

a Biodistribution of ^{64}Cu-DOTA-GX1 in U87MG tumor bearing athymic nude mice at 24 h with and without co-injection of 20 mg/kg of GX1 peptide as a blocking agent (n=3/group). **b** Ratio of tumor-to-major organs (liver, kidney, and muscle) based on the biodistribution data. Error bar was calculated as the standard deviation (n=3/group).

Table 1

Data from the HPLC analysis of metabolic stability of ^{64}Cu-DOTA-GX1 peptide in mouse blood sample, urine, liver, and kidney homogenates at 1 h pi

	Blood	Urine	Liver	Kidney
HPLC Analysis [%] (n=2)				
Met 1	16.1±3.0	18.1±2.5	49.6±1.7	35.6±1.3
Met 2	8.7±3.5	n.d.	12.2±2.5	n.d.
Intact Tracer	75.2±3.8	81.9±1.8	38.2±2.2	64.4±1.3

n.d. Not detectable